ACCEPTED VERSION

Peipei Jia, Depeng Kong, Heike Ebendorff-Heidepriem
Resist-free nanoimprinting on optical fibers for plasmonic optrodes

Final publication at: http://dx.doi.org/10.1016/j.apmt.2020.100751

http://hdl.handle.net/2440/126775

Resist-free nanoimprinting on optical fibers for plasmonic optrodes

Peipei Jia [a,b], Depeng Kong [c], Heike Ebendorff-Heidepriem [a,]*

[a]ARC Centre of Excellence for Nanoscale BioPhotonics (CNBP)
Institute for Photonics and Advanced Sensing (IPAS), School of Physical Sciences
The University of Adelaide, Adelaide 5005, Australia.
[b]Shenzhen Topmembrane Technology Co., Ltd.
Shenzhen 518000, China
[c]Key Laboratory of Transient Optics and Photonics
Xi'an Institute of Optics and Precision Mechanics of CAS (XIOPM)
Shannxi 710119, China

* Corresponding author. E-mail: heike.ebendorff@adelaide.edu.au

Abstract: Nanostructure patterning on optical fibers enables miniaturized optrodes for photonic and plasmonic applications. Here we report a direct nanoimprint technique to produce high-quality nanostructure arrays on optical fiber endfaces. It has only one single step: imprinting optical fiber tips against a mold with nanostructures at the elevated temperature. This new method abandons resist used in traditional fiber-imprinting methods. Hundreds of fibers can be shaped simultaneously with one mold within minutes. The imprinted nanostructure arrays on optical fibers are transformed into plasmonic optrodes through metal deposition. Variation of imprint depths and mold patterns allows tailoring of the plasmonic resonances of these nanostructure arrays for high-performance refractometric sensing and on-fiber polarization. The sensitivity of 690 nm/RIU and figure of merit of 50 are both among the highest values for similar plasmonic nanostructure arrays. This resist-free nanoimprint paves the way towards a low-cost and high-throughput realization of plasmonic optrodes and their wide applications.

Keywords: nanoimprint, nanostructure arrays, resist-free, optical fibers, plasmonics

1. Introduction

Optical fibers provide an inherently light-coupled microscopic platform for nanophotonics and plasmonics [1]. Realization of functional nanostructure arrays on optical fiber tips allows for their application in remote sensing and spectroscopy. As the fiber

manufacture technique limits the possible structures and materials of optical fibers, the post-fabrication provides an alternative way of achieving novel nanostructure arrays on fiber tips. For example, various two-dimensional metasurfaces have been achieved on optical fiber endfaces for beam steering, light focusing and polarization [2-5]. Such integration far extends the scope of fiber-optics based photonic and plasmonic devices in chemistry, medicine and biotechnology [6-7].

However, precise fabrication of nanostructure arrays on fiber facets is challenging due to the small cross section and large aspect ratio of optical fibers, which are incompatible with many traditional manufacture techniques. The modest readiness of the current integration technology (e.g. high cost, poor quality control and low repeatability) results in barriers to their real-world applications. On-fiber patterning has been realized with advanced techniques such as electron-beam lithography (EBL) for concentric nanorings and hybrid nanohole arrays [8-9] and focused ion-beam (FIB) milling for nanoaperture, nanodisk and nanorod arrays [10-12]. These methods either require special and complex apparatus to host and align the optical fiber or suffer from low yield of nanostructures. Alternatively, other techniques separate pattern generation from optical fibers and then transfer the as-prepared nanoantenna structures onto the fiber tips [13-14]. However, the transfer process is inherently serial and thus offsets the advantage of high-throughput in the patterning stage.

In contrast, nanoimprint has provided a simple way of large-area interface molding by mechanical deformation of resist on fiber tips [15-19]. For example, an efficient parallel-imprinting method loaded several fibers into an array of grooves for imprinting against a mold [20]. Still, inherent shortcomings exist: (i) the use of photoresist as structure host complicated the fabrication process. Despite using anti-adhesion layers, it was difficult to release the cured structures from the mold; (ii) the throughput was limited by specially designed fiber holders. For instance, the number of grooves in this batch method eventually determined the amount of

imprinted fibers in one production cycle. Moreover, the grooves have to space each fiber to prevent them from sticking together after resist curing.

Here we exploit a nanoimprint technique to realize functional nanostructure arrays on optical fiber endfaces. It has only one single-step: direct imprinting optical fiber tips against a mold with negative nanostructures at the elevated temperature. The following metal deposition transforms these nanostructure arrays into plasmonic structures. This new method abandons resist used in previous fiber-imprinting techniques. The imprinting occurs on the interface of the mold-fiber instead of the mold-resist, enabling mass production. To show its capability, various nanostructure arrays are imprinted on plastic optical fiber tips with high precision and quality. By applying different pressures, we can tune the imprint depth whereby the plasmonic resonance coupled between the imprinted structures can be modulated. We also demonstrate on-fiber polarization by imprinting nanoslits on fiber tips. The double-strip array reveals a Fano profile due to resonance mode coupling. Our resistless nanoimprint technique offers a practical and scalable solution for realizing nanostructure arrays on optical fibers for plasmonic applications.

2. Material and methods

2.1 Fiber polishing

One hundred parallel-arranged optical fibers were packaged in a plastic sleeve, held by a homemade hand polish puck. The puck can keep the axes of the fibers perpendicular to the lapping film during polishing. Regular fiber polishing procedures were conducted to obtain flat and smooth fiber facets. Lapping films of different grit sizes were used in one process, and flushed with deionized water during polishing.

2.2 Refractive index sensitivity measurement

Refractive index solutions were prepared by adding NaCl into deionized water to obtain various concentrations (5%, 10%, 15% and 20%) with refractive index (1.3418,

15

1.3505, 1.3594, and 1.3684, respectively). The imprinted optical fiber was equipped into a home-made flow cell, through which the solutions were injected sequentially. The light transmitted through the imprinted nanostructures was collected by another face-to-face configured fiber coupled to a spectrometer (USB4000, Ocean Optics). All transmission spectra were recorded by averaging acquisitions and the refractive index sensitivities are calculated by linearly fitting peak or trough shifts in transmission.

2.3 FDTD simulation

Although the round shape of fiber endface resulted in the unequal length of adjacent nanostrips, it is safe to ignore this very limited difference in simulation. 2D simulation was performed along the cross-section plane of the nanostrips using a commercial software, FDTD solutions (Lumerical). The simulation area contained one unit of strip structures and a uniform mesh size of 2 nm along x and z directions was used. We set periodic boundary conditions for x direction of the simulation region and perfectly matched layer boundary conditions for the z direction. The refractive index of the PMMA fiber was set to be 1.49.

2.4 In-line polarization measurement

The white light was polarized by a linear polarizer (LPVIS100, Thorlabs) mounted in an indexed rotation mount. The polarized light was then coupled into the imprinted optical fiber from the distal end without structures. The light through the imprinted nanostructures was collected by another face-to-face configured fiber to record the transmission spectra for the extinction ratio calculation.

3. Results and discussion

3.1 Procedure of nanoimprinting optical fibers

Figure 1a illustrates the schematic of our optical fiber nanoimprint setup. To demonstrate the viability of our nanoimprint method, we choose a plastic optical fiber consisting of a PMMA core with glass transition (Tg) of around 115 ⁰C (Figure S1). Hundreds

15

of fibers can be shaped with one mold in a single imprinting cycle within minutes. Because

our direct imprinting requires no resist, the number of fibers that can be accommodated only

depends on the size of the Si imprint mold. For instance, a bundle of optical fibers are

packaged in a plastic sleeve and polished before imprinting. The Si mold with nanostructures

is heated on a hot plate to a temparature of 128 ºC. Then, by pushing the fibers against the

mold with certain pressure and retracting them after a few seconds, the designed geometries

are imprinted into the fiber tips. After cooling down to room temperature, the imprinted fibers

can be easily detached from the mold due to its low adhesion to Si. By gold deposition on the

tips, these imprinted arrays are turned into plasmonic nanostructures. Each individual fiber

can be isolated from the bundle afterwards without damage (Figure 1b). These fibers reflect

bright colors due to the strong resonance from the periodic metal nanostructures (Figure 1c).

In comparison, color is only visible in the area subject to the Bragg condition before

metallization.
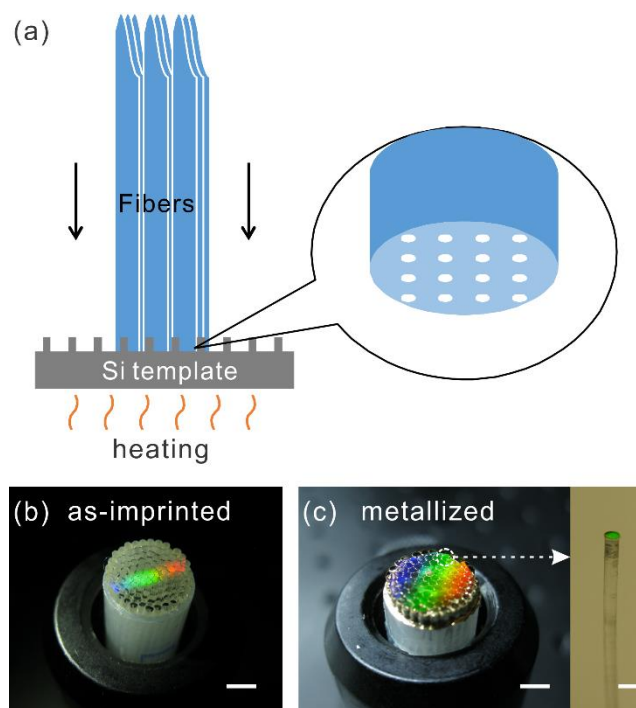
Fig. 1. Nanoimprinting optical fibers. (a) Schematic of the optical fiber imprint setup. (b) A bundle of as-imprinted plastic optical fibers. Scale bar: 3 mm. (c) Imprinted optical fibers with 75 nm gold deposited on the tips. The fiber diameter is 0.75 mm. Scale bars: 3 mm in left and 1mm in right.

3.2 Characterization of imprinted nanostructures

The fiber facets can be shaped into typical arrays of nanowells, nanodots and nanoslits by using Si molds (LightSmyth Technologies) with complementary structures respectively (Figure 2). These arrays extend to the edge of the fibers and maintain spatial uniformity and high quality across the entire tips. The minimum feature (e.g. Figure 2c) can reach below 50 nm, depending on the Si molds. In thermal nanoimprint, the temperature is usually 70-90°C above the Tg of resist [21]. However, above the Tg and below the melting point of a thermoplastic, both its Young's modulus and viscosity will drop by several orders of magnitude compared to the respective values at room temperature [22]. Thus, the imprint temperature is critical to control the geometry and morphology of the nanostructures. In our experiment, imprinting at the temperature of about 135°C results in serious surface roughness and undesired structures, plus significant deformation of the fiber tip. In contrast, imprinting at 128°C (about 10°C above the Tg) only yields about 5% bulge in diameter at the fiber tip due to squeezing the polymer off the fiber axis.
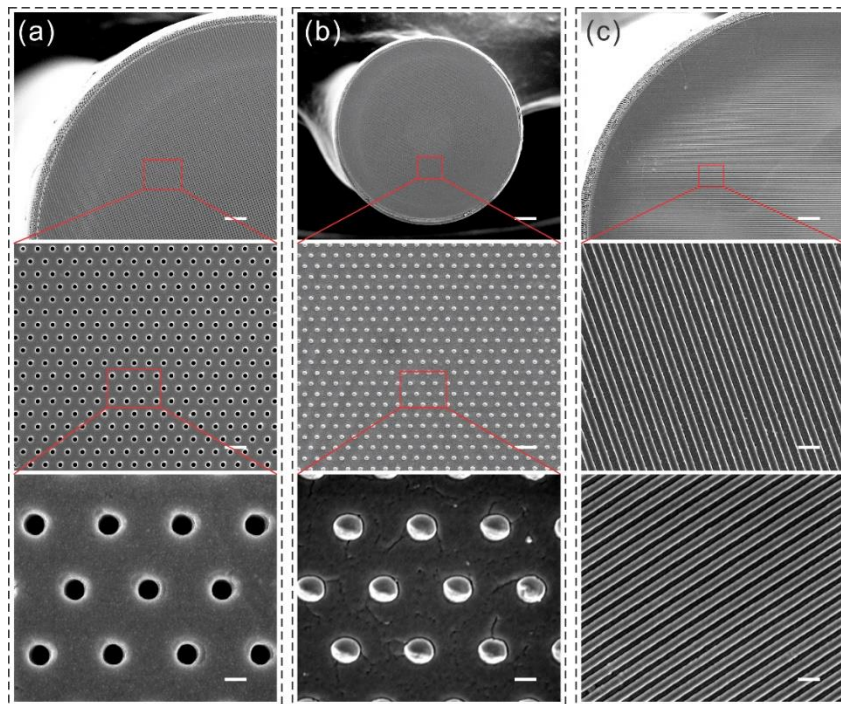

Fig. 2. SEM images of imprinted nanostructures on optical fiber endfaces: (a) nanowell array (200 nm diameter, 700 nm pitch) (b) nanodot array (250nm diameter, 700 nm pitch), and (c) nanoslit arrays (the top and center: 200 nm width, 500 nm pitch; the bottom: 45 nm width,

150 nm pitch). From top to bottom, scale bars: (a) 0.5 mm, 1 µm, 200 nm; (b) 1 mm, 1 µm, 200 nm; (c) 0.4 mm, 700 nm, 200 nm;

3.3 Plasmonic resonance coupling modulation

By varying the imprint pressure, we can control the depth of the imprinted nanostructure (Figure 3a). There is a linear dependence of depth on presusre in the case of nanowell imprinting, as shown in Figure 3b. The nanowell depth can approach the same height of the nanoposts on the mold when the pressure reaches 3.0 MPa. Additionally, we find that the cross section of nanowells in the fiber facet plane increases as the depth decrease. The diameter of the deepest nanowells (~205 nm) is close to that of the used nanopost mold (195 nm); however, the nanowells of 30 nm depth have a much larger cross section (~260 nm). The reason is probably the shear-thinning viscosity behaviour of polymer, resulting in 'spring-back' phenomena. When the heated nanopost stamp is moved into the fiber tip, the imprinted PMMA is under pressure whereby the polymer chains are depressed. When removing the pressure, the chains spring back. Therefore, larger pressure leads to more hole shrinkage [23].
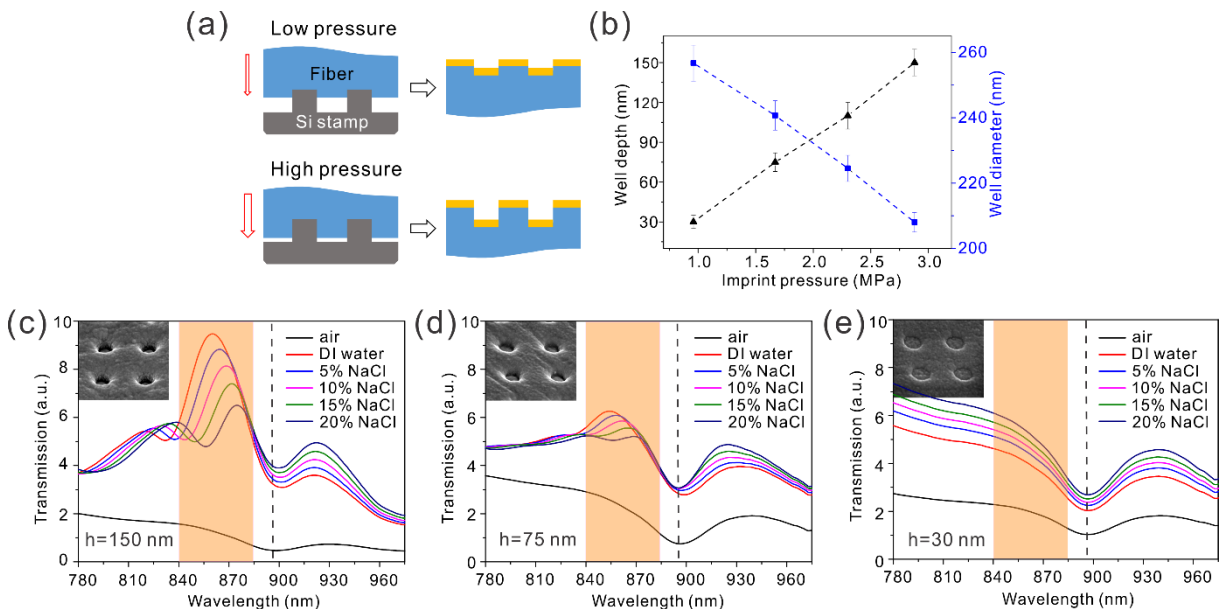
Fig. 3. Depth control of nanoimprint. (a) Schematic of imprint depth control: low pressure for shallow wells, high pressure for deep wells. (b) Dependence of nanowell depth and diameter on imprint pressure. Plasmonic resonance coupling modulation through varying imprint depth: (c) 150nm, (d) 75 nm and (e) 30 nm. Transmissions of the imprinted nanowells on fibers are measured after metallization in air, DI water and NaCl solutions for calculation of refractive index sensitivity. All transmission figures have the same arbitrary unit. The colored

15

areas highlight the wavelength range for spectral feature comparison. The dash lines indicate the Rayleigh cut-off wavelength. Insets of (c-e) are SEM images of the gold nanowell arrays.

For the imprinted nanowells, gold deposition (75 nm thick) perpendicular to the fiber facet creates a nanohole array film on the relief region and a second level of a nanodisk array at the bottom. Imprint depth varies the distance between the two arrays whereby their resonance coupling can be modulated [24], as evidenced by the comparison of transmision peaks between 840 nm and 885 nm in Figure 3c-e. For the deepest imprinting (~150 nm), strong coupling resonance is obtained (Figure 3c); the shallower the nanowells are, the weaker the resonance is (Figure 3d). For low pressure imprinting with 1.0 MPa, the two arrays form a continuing film with only shallow nanowells (~30 nm depth). The connection of the nanohole array and nanodisk array short-circuits the capacitively coupled gold disks and holes, and thus no obvious resonance exists (Figure 3e).

Plasmonic resonances are sensitive to the dielectric condition at the surface of the metal nanostructures. The refractive index sensitivities of these plasmonic fibers are determined by using NaCl solutions with different concentrations. The multiple maxima and minima in the spectra of Figure 3c are possibly due to the excitation of multiple modes of resonances. As the used optical fibers are multiple-mode fibers, the incident light can excite other modes of resonances beyond that from the normal incidence, leading to multiple peaks/troughs. Although the resonance peak intensity changes with imprint depth in the colored wavelength range in Figure 3c-e, their refractive index sensitivities, i.e., peak wavelength shift (nm) per refractive index unit (RIU), are all around 400 nm/RIU, which is lower than the theoretical value of 600 nm/RIU for this kind of nanostructure arrays at this wavelength range [25]. This is probably due to the presence of Rayleigh cut-off at 894 nm, corresponding to the nanohole array with 600 nm pitch on the PMMA substrate (refractive index 1.49) [26]. As the resonance shifts to longer wavelength, it is gradually coupled with this cut-off. This coupling hinders the shift of the peak, leading to a lower sensitivity. In

comparison, the troughs around 840 nm achieve a high sensitivity of 690 nm/RIU (Figure 3c). This value exceeds the previously reported values of the similar nanostructure arrays imprinted on planar substrates [24,27]. With a full width at half maximum (FWHM) of 13.7 nm, the figure of merit (FOM, defined as sensitivity/FWHM) reaches as high as 50, which is among the highest values for plasmonic nanostructure arrays [25] and larger than the previously reported plasmonic fiber sensors (FOM<16) [8-12].

3.4 On-fiber polarization

In-line optical fiber polarization can be realized through imprinting a nanoslit array on the fiber endface. By gold deposition, gold thin strips are formed on the bottom of the slits as well as on the terrace between them. This double-layer nanostrip array is designed to pass transverse-magnetic (TM) polarized light (perpendicular to nanostrips in the fiber facet plane) while blocking the transverse-electric (TE) polarization. The TM transmission spectrum reveals a Fano-shape profile of two partially overlapped peaks (Figure 4a). The extinction ratio between TM and TE transmission (Figure 4b) can reach about 100 by using the mold with the duty cycle of 60% (the ratio of 300 nm width over 500 nm pitch).
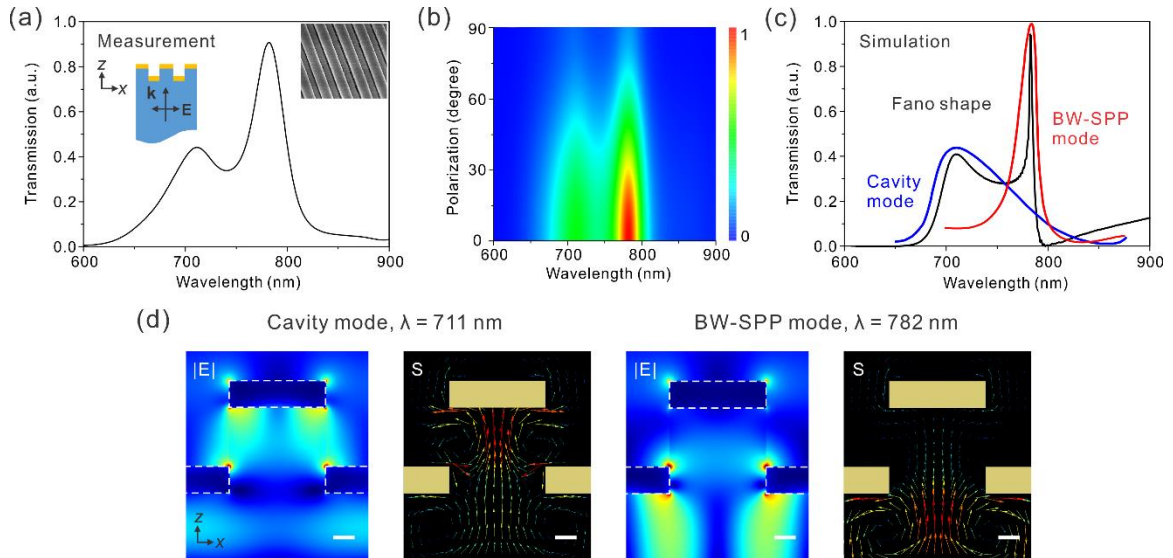
Fig. 4. In-line optical fiber polarization. (a) Measured TM transmission of gold nanostrips on the imprinted optical fiber. Inset, schematic of optical configuration with the direction of the TM-polarized incident light with E and k vectors and SEM image of the nanostrips. (b) Transmission spectra measured with polarized incident light from TM (0°) to TE (90°). (c) Simulated transmission spectrum (black) with Fano-shape profile due to coupling between

15

cavity mode (blue) and BW-SPP mode (red). (d) Electric field distribution (|E|) and Poynting vector mapping (S) for cavity mode at 711 nm and BW-SPP mode at 782 nm in FDTD simulation, respectively. Scale bars: 50 nm.

To understand the physics behind the spectral features, we have conducted finite-difference time-domain (FDTD) simulation to investigate the optical properties of the double-layer nanostrip array. The simulated spectrum reproduces the Fano-shape profile of TM transmission: a sharp peak coupled with one broadband peak (Figure 4c). The measured and calculated spectra are in good agreement considering two minor differences: first, both of the measured peaks are broader than the simulation predicts; secondly, the experimental minimum between two peaks blueshifts compared with the simulated value. One probable reason is that the ideal rectangular cross sections of the nanostrips in the simulation is simplified from the actual nanostrip shape. Such deviation could change the line width and the resonance coupling. The difference in dielectric functions between simulation and experiment can also result in different peak widths.

The simulated field mappings disclose the intrinsic resonance properties as shown in Figure 4d. The electric field distributions indicate that the broad transmission peak at 711 nm is mediated by a cavity mode between the two layers of the strip array, which satisfies the Fabry-Perot condition [28]. Poynting vector mapping reveals that the bottom strips collect the incident light like an antenna and induce an enhanced electrical field, which is further coupled to the top strips, resulting in a resonance between them. In comparison, the electric field of the sharp peak at 782 nm is mostly confined to the gold surface and gradually extends to the surrounding medium. This field profile indicates that surface plasmon (SP) are excited on the bottom strips. Thus the narrow peak can be attributed to the Bloch wave-surface plasmon polaritons (BW-SPP), occurring at the wavelength when the Bragg condition is satisfied [29]:

$\lambda(n, i) = \frac{P}{i} \pi \text{Re} \left\{ \left(\frac{\varepsilon_m n^2}{\varepsilon_m + n^2} \right)^{1/2} \right\}$, where i is the resonant order, P is the pitch of the nanostrip

array, ε_m is the dielectric constant of gold and n is the refractive index of PMMA. Eventually

the interaction between the cavity resonance and the BW-SPP mode leads to a Fano-shape resonance. This two-layer structure provides two advantages of Fano resonances: it enhances the cavity mode resonance due to a higher reflection at the top interface; and it increases the asymmetrical factor because the longitudinal cavity mode is efficiently coupled to lateral BW-SPP mode [28].

4. Conclusions

In conclusion, we have developed a resist-free and high-throughput nanoimprint technique for fabrication of nanostructure arrays on optical fibers. The plastic optical fiber endfaces can be imprinted into various nanostructure arrays in minutes. The imprinted nanostructure arrays can be transformed into functional plasmonic devices by metallization. By varying the imprint depth and using molds with different geometries, the properties of the plasmonic fibers can be modulated. Compared to previous imprint methods, the direct nanoimprint not only eliminates the need of resist, but also improves the fabrication efficiency. The imprinting occurs on the interface of the mold-fiber instead of the mold-resist, enabling an elaborate procedure without sticking problem. In addition, the imprinted fibers are packaged in a plastic sleeve into a two-dimensional array comparable to the template size, leading to full use of the nanostructures on the template. Thus, hundreds of fibers can be shaped simultaneously with one mold in one simple imprint cycle within minutes. This technique is promising to be further scaled up and to expand the capability of nanostructure array shaping on optical fiber endfaces for more photonic and plasmonic applications.

Declaration of Competing Interest

The authors declare that they do not have any conflict of interests.

Microscopy, the South Australian node and Optofab node of the Australian National Fabrication Facility (ANFF) utilizing Commonwealth and SA State Government funding.

Supporting Information

Supplementary Information of this article can be found in the online version.

References

[1] G. Kostovski, P.R. Stoddart, A. Mitchell, The optical fiber tip: an inherently light-coupled microscopic platform for micro- and nanotechnologies, Adv Mater, 26 (2014) 3798-3820.

[2] M. Principe, M. Consales, A. Micco, A. Crescitelli, G. Castaldi, E. Esposito, V. La Ferrara, A. Cutolo, V. Galdi, A. Cusano, Optical fiber meta-tips, Light: Science & Applications, 6 (2017) e16226-e16226.

[3] J. Yang, I. Ghimire, P.C. Wu, S. Gurung, C. Arndt, D.P. Tsai, H.W.H. Lee, Photonic crystal fiber metalens, Nanophotonics, 8 (2019) 443.

[4] J. Flannery, R. Al Maruf, T. Yoon, M. Bajcsy, Fabry-Pérot Cavity Formed with Dielectric Metasurfaces in a Hollow-Core Fiber, ACS Photonics, 5 (2018) 337-341.

[5] M. Juhl, J.P.B. Mueller, K. Leosson, Metasurface Polarimeter on Optical Fiber Facet by Nano-Transfer to UV-Curable Hybrid Polymer, IEEE Journal of Selected Topics in Quantum Electronics, 25 (2019) 1-7.

[6] X.-d. Wang, O.S. Wolfbeis, Fiber-Optic Chemical Sensors and Biosensors (2013–2015), Anal Chem, 88 (2016) 203-227.

[7] P. Vaiano, B. Carotenuto, M. Pisco, A. Ricciardi, G. Quero, M. Consales, A. Crescitelli, E. Esposito, A. Cusano, Lab on Fiber Technology for biological sensing applications, Laser & Photonics Reviews, 10 (2016) 922-961.

[8] S. Feng, S. Darmawi, T. Henning, P.J. Klar, X. Zhang, A Miniaturized Sensor Consisting of Concentric Metallic Nanorings on the End Facet of an Optical Fiber, Small, 8 (2012) 1937-1944.

[9] M. Consales, A. Ricciardi, A. Crescitelli, E. Esposito, A. Cutolo, A. Cusano, Lab-on-Fiber Technology: Toward Multifunctional Optical Nanoprobes, ACS Nano, 6 (2012) 3163-3170.

[10] A. Dhawan, J.F. Muth, D.N. Leonard, M.D. Gerhold, J. Gleeson, T. Vo-Dinh, P.E. Russell, Focused ion beam fabrication of metallic nanostructures on end faces of optical fibers for chemical sensing applications, Journal of Vacuum Science & Technology B: Microelectronics and Nanometer Structures Processing, Measurement, and Phenomena, 26 (2008) 2168-2173.

[11] M. Sanders, Y. Lin, J. Wei, T. Bono, R.G. Lindquist, An enhanced LSPR fiber-optic nanoprobe for ultrasensitive detection of protein biomarkers, Biosensors and Bioelectronics, 61 (2014) 95-101.

[12] E.J. Smythe, E. Cubukcu, F. Capasso, Optical properties of surface plasmon resonances of coupled metallic nanorods, Optics Express, 15 (2007) 7439-7447.

[13] E.J. Smythe, M.D. Dickey, G.M. Whitesides, F. Capasso, A technique to transfer metallic nanoscale patterns to small and non-planar surfaces, ACS Nano, 3 (2009) 59-65.

[14] E.J. Smythe, M.D. Dickey, J. Bao, G.M. Whitesides, F. Capasso, Optical Antenna Arrays on a Fiber Facet for in Situ Surface-Enhanced Raman Scattering Detection, Nano Lett, 9 (2009) 1132-1138.

[15] S. Scheerlinck, D. Taillaert, D.V. Thourhout, R. Baets, Flexible metal grating based optical fiber probe for photonic integrated circuits, Appl Phys Lett, 92 (2008) 031104.

[16] S. Scheerlinck, P. Dubruel, P. Bienstman, E. Schacht, D.V. Thourhout, R. Baets, Metal Grating Patterning on Fiber Facets by UV-Based Nano Imprint and Transfer Lithography Using Optical Alignment, Journal of Lightwave Technology, 27 (2009) 1415-1420.

[17] G. Kostovski, D.J. White, A. Mitchell, M.W. Austin, P.R. Stoddart, Nanoimprinted optical fibres: Biotemplated nanostructures for SERS sensing, Biosensors and Bioelectronics, 24 (2009) 1531-1535.

[18] G. Calafiore, A. Koshelev, F.I. Allen, S. Dhuey, S. Sassolini, E. Wong, P. Lum, K. Munechika, S. Cabrini, Nanoimprint of a 3D structure on an optical fiber for light wavefront manipulation, Nanotechnology, 27 (2016) 375301.

[19] J. Viheriala, T. Niemi, J. Kontio, T. Rytkonen, M. Pessa, Fabrication of surface reliefs on facets of singlemode optical fibres using nanoimprint lithography, Electronics Letters, 43 (2007) 150-151.

[20] G. Kostovski, U. Chinnasamy, S. Jayawardhana, P.R. Stoddart, A. Mitchell, Sub-15nm Optical Fiber Nanoimprint Lithography: A Parallel, Self-aligned and Portable Approach, Advanced Materials, 23 (2011) 531-535.

[21] L.J. Guo, Recent progress in nanoimprint technology and its applications, Journal of Physics D: Applied Physics, 37 (2004) R123-R141.

[22] L.J. Guo, Nanoimprint Lithography: Methods and Material Requirements, Advanced Materials, 19 (2007) 495-513.

[23] H. Ebendorff-Heidepriem, T.M. Monro, M.A. van Eijkelenborg, M.C.J. Large, Extruded high-NA microstructured polymer optical fibre, Optics Communications, 273 (2007) 133-137.

[24] K. Nakamoto, R. Kurita, O. Niwa, T. Fujii, M. Nishida, Development of a mass-producible on-chip plasmonic nanohole array biosensor, Nanoscale, 3 (2011) 5067-5075.

[25] P.P. Jia, J. Yang, Universal sensitivity of propagating surface plasmon resonance in nanostructure arrays, Optics Express, 23 (2015) 18658-18664.

[26] J.M. McMahon, J. Henzie, T.W. Odom, G.C. Schatz, S.K. Gray, Tailoring the sensing capabilities of nanohole arrays in gold films with Rayleigh anomaly-surface plasmon polaritons, Optics Express, 15 (2007) 18119-18129.

[27] M. Zhang, M. Lu, C. Ge, B.T. Cunningham, Plasmonic external cavity laser refractometric sensor, Optics Express, 22 (2014) 20347-20357.

[28] K.-L. Lee, J.-B. Huang, J.-W. Chang, S.-H. Wu, P.-K. Wei, Ultrasensitive Biosensors

Using Enhanced Fano Resonances in Capped Gold Nanoslit Arrays, Scientific Reports, 5

(2015) 8547.

[29] S.-H. Chang, S.K. Gray, G.C. Schatz, Surface plasmon generation and light transmission
by isolated nanoholes and arrays of nanoholes in thin metal films, Optics Express, 13 (2005)
3150-3165.